Production and recovery of defects in phosphorus-implanted ZnO

Z. Q. Chen,[a] A. Kawasuso, Y. Xu, and H. Naramoto
Advanced Science Research Center, Japan Atomic Energy Research Institute, 1233 Watanuki, Takasaki, Gunma 370-1292, Japan

X. L. Yuan and T. Sekiguchi
Nanomaterials Laboratory, National Institute for Materials Science, 1-2-1 Sengen, Tsukuba, Ibaraki 305-0047, Japan

R. Suzuki and T. Ohdaira
National Institute of Advanced Industrial Science and Technology, 1-1-1 Umezono, Tsukuba, Ibaraki 305-8568, Japan

(Received 24 May 2004; accepted 1 October 2004; published online 15 December 2004)

Phosphorus ions were implanted in ZnO single crystals with energies of 50–380 keV having total doses of 4.2×10^{13}–4.2×10^{15} cm^{-2}. Positron annihilation measurements reveal the introduction of vacancy clusters after implantation. These vacancy clusters grow to a larger size after annealing at a temperature of 600 °C. Upon further annealing up to a temperature of 1100 °C, the vacancy clusters gradually disappear. Raman-scattering measurements reveal the enhancement of the phonon mode at approximately 575 cm^{-1} after P^+ implantation, which is induced by the production of oxygen vacancies (V_O). These oxygen vacancies are annealed out up to a temperature of 700 °C accompanying the agglomeration of vacancy clusters. The light emissions of ZnO are suppressed after implantation. This is due to the competing nonradiative recombination centers introduced by implantation. The recovery of the light emission occurs at temperatures above 600 °C. The vacancy-type defects detected by positrons might be part of the nonradiative recombination centers. The Hall measurement indicates an *n*-type conductivity for the P^+-implanted ZnO layer, suggesting that phosphorus is an amphoteric dopant.
 [DOI: 10.1063/1.1821636]

I. INTRODUCTION

Since the production of large area ZnO single crystals,[1] there has been a growing interest in this material in recent years. This is due to its wide band gap (3.4 eV) and large exciton binding energy (60 meV), which enables its potential application in short wavelength-light emitting diodes and lasers.[2,3] However, a disadvantage of this material is the inability to reproduce a *p*-type conductivity. While some authors have reported the successful fabrication of a *p*-type ZnO by either doping with nitrogen[4,5] or codoping with Ga +N,[6,7] many other researchers have failed.[8–11] There are several probable reasons for such a *p*-type difficulty; for example, low solubility of dopants, self-compensation by native donor-type defects, deep acceptor levels that make it difficult to be ionized at room temperature, or the formation of an electrically inactive state. Among these factors, defects play a major role because they might not only compensate for the acceptors but also form stable complexes with acceptor dopants and convert them to an electrically inactive state.

Ion implantation has become a necessary processing tool for semiconductor device fabrication. This method can incorporate dopants in the selected region in a controllable amount. During the slowing down of the implanted ions, various defects are also inevitably created. These defects strongly affect the activation of dopants during subsequent annealing. They may also affect other electrical and optical properties and cause the unexpected degradation of semiconductor devices. The study of the production and recovery process of these defects is therefore very important for a successful doping. There have been a number of studies on the defects induced by ion implantation in ZnO using Rutherford backscattering,[12,13] photoluminescence and cathodoluminescence,[14] deep-level transient spectroscopy,[15] secondary-ion-mass spectrometry,[16] and other electrical characterization methods.[17,18] In addition to these methods, positron annihilation spectroscopy has recently emerged as a powerful tool for the study of vacancy-type defects in semiconductors.[19] Due to the Coulomb repulsion from the positive-ion cores, positrons are more likely to be trapped by open volume defects where atoms are missing. The annihilation characteristics of the trapped positrons show differences from the defect-free bulk state, i.e., a longer positron lifetime and narrower Doppler broadening of the annihilation gamma rays. Using a monoenergetic slow positron beam, it is possible to study the defects in the surface and subsurface regions up to a few micron below the surface.[20]

In this paper, we implanted phosphorus as a possible *p*-type dopant in ZnO. On the basis of a recent theoretical calculation, phosphorus at an oxygen site (P_O) is expected to be a deep acceptor. However, phosphorus in ZnO is also reported to be an amphoteric dopant.[21] It may replace O to form acceptors or replace Zn to form donors.[21] So far, few papers have reported successful *p*-ZnO growth by phosphorus doping,[22] whereas the results from other studies have

[a]Electronic mail: chenzq@taka.jaeri.go.jp

found an *n*-type conductivity.[23,24] Therefore, it is worthwhile to reexamine the phosphorus doping in ZnO by the ion implantation technique. Both positron annihilation and Raman-scattering measurements were employed to obtain comprehensive information regarding defects and their thermal evolution. The optical properties before and after implantation and subsequent annealing were monitored by cathodoluminescence, and the conductivity of the P^+-implanted ZnO layer was confirmed by the Hall measurement after final annealing.

II. EXPERIMENT

Hydrothermal-grown undoped ZnO single crystals with a double-sided polished surface were purchased from the Scientific Production Company (SPC Goodwill). These samples exhibit an *n*-type conductivity with an electron concentration of approximately 5.7×10^{12} cm^{-3}. Ion implantation was performed at room temperature using a 400-keV ion implanter. P^+ ions with seven different energies ranging from 50 to 380 keV were implanted in the Zn face of the ZnO samples. By choosing an appropriate dose for each ion energy, a box-shaped implantation profile can be formed after such a multiple-step implantation.[25] Detailed information regarding the multiple-step implantation is presented in our recent paper.[25] In this work, we used the same dose for each energy as in Ref. 25. Therefore, the total doses were 4.2×10^{13}, 4.2×10^{14}, and 4.2×10^{15} cm^{-2}; and the beam flux was 1.2×10^{12} $cm^{-2}\,s^{-1}$. The TRIM calculation[26] revealed the thickness of the implantation box layer to be approximately 450 nm. The implanted samples were isochronally annealed up to a temperature of 1100 °C in a nitrogen atmosphere for a period of 30 min at each temperature.

The Doppler broadening of positron annihilation was measured using a high-purity Ge detector with an energy resolution of approximately 1.3 keV at 511 keV. A slow positron beam was used with positron energies varying from 0.2 to 30 keV. The *S* parameter was used to characterize the measured spectra, which is the ratio of the total counts in the central region (511 ± 0.77 keV) to the total area under the 511 annihilation peak (511 ± 8.5 keV). In this paper, the *S* parameters were normalized to the value in the deep bulk region of the unimplanted sample. Therefore, a value of $S>1$ implies the presence of vacancy defects. A pulsed slow positron beam at the National Institute of Advanced Industrial Science and Technology was also used to measure positron lifetime.[27] Micro-Raman-scattering measurements were conducted using the NANOFINDER spectrometer in the wavenumber range of 200–800 cm^{-1}. The 488.0-nm line of an Ar^+-ion laser was used for excitation, and the incident laser power was ~1 mW. The measurement time for each spectrum was 60 s. Cathodoluminescence measurements were conducted using a scanning electron microscope (TOPCON DS130) attached with a beam blanking system.[28] In this study, the electron-beam energy and current for excitation were 5 keV and 1 nA, respectively. The measurement time for each spectrum was 5 s. Hall measurements were performed using the van der Pauw method.[29] The ohmic contacts were fabricated by evaporating gold at the four symmetrical corners of the samples. All the above measurements were conducted at room temperature.

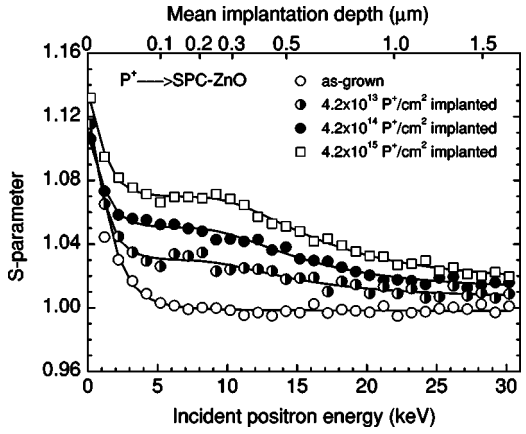

FIG. 1. *S* parameter as a function of incident positron energy measured for ZnO samples before and after P^+ implantation. The solid lines are drawn as a guide to the eye.

III. RESULTS AND DISCUSSION

A. Defect characterizations

Figure 1 presents the Doppler broadening *S* parameter as a function of incident positron energy measured for the as-grown and P^+-implanted ZnO. For the as-grown sample, the *S* parameter decreases gradually with an increasing positron energy and becomes constant at $E>7$ keV. The higher *S* parameter at low energy is due to the positron annihilation at surface states. With increasing incident energy, the positron annihilates in the deep bulk region. The positron lifetime measurement reveals a single lifetime of approximately 182 ± 1 ps in the bulk region ($E=10$ keV), which is close to the bulk lifetime reported in our earlier studies.[30] This confirms that in the unimplanted sample, there are fewer vacancies that trap positrons.

After P^+ implantation, the *S* parameters exhibit an increase and maintain a constant value in the energy range of 4–11 keV for each dose. This indicates the introduction of vacancy defects after P^+ implantation. The plateau region corresponds to the box-shaped implantation layer, suggesting a homogeneous defect distribution in the box layer. The *S* parameter increases up to approximately 1.07 at the highest dose. The positron lifetime spectrum measured with an incident positron energy of 7 keV reveals two lifetime components: $\tau_1=209\pm22$ ps, and $\tau_2=343\pm16$ ps, after P^+ implantation at a dose of 4.2×10^{15} cm^{-2}. The first component is the average lifetime of positrons annihilated at free and at trapped states with monovacancies, while the second lifetime can be attributed to the positron annihilation at the vacancy clusters. The intensities of the first and second components are $37\pm10\%$ and $63\pm10\%$, respectively. This means that these defects are mostly vacancy clusters, with few coexisting monovacancies. According to the theoretical calculation,[25] the size of the vacancy cluster is close to that of the hexavacancy (V_6).

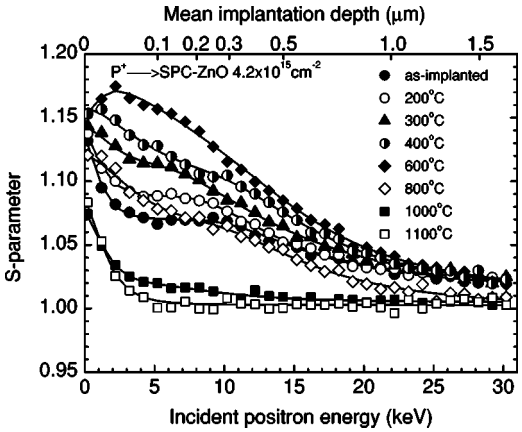

FIG. 2. Annealing behavior of the *S*-*E* curves measured for the P^+-implanted ZnO with dose of 4.2×10^{15} cm^{-2}. The solid lines are drawn as a guide to the eye.

Figure 2 shows some selected *S*-*E* curves for the P^+-implanted sample at a dose of 4.2×10^{15} cm^{-2} after annealing at different temperatures. The *S* parameters first exhibit an increase with temperature up to 600 °C, followed by a decrease; finally, the *S*-*E* curve approaches that of the unimplanted sample. After annealing, the *S* parameters are no longer constant in the implanted region. This might be due to the defect diffusion, and therefore, a change in the depth distribution of defects. We calculated the average *S* parameter from the integrated Doppler spectra measured in the energy range of 5–8 keV (0.1–0.2 μm), which corresponds to the central region of the implanted box layer. The change in the average *S* parameter as a function of annealing temperature is shown in Fig. 3, which exhibits two processes. First, a continuous increase in the *S* parameter can be observed after annealing below 600 °C. This is due to the increase of the vacancy cluster size through the agglomeration of small vacancies, which is due to the fact that these vacancies become mobile in this temperature range. It is notable that the *S* parameters increase to a high value of more than 1.15 at 600 °C. This implies that the vacancy clusters grow very large, or even that microvoids are possibly formed. Second, after annealing at temperatures above 600 °C, the *S* parameters begin to drop, and they gradually decrease to the bulk

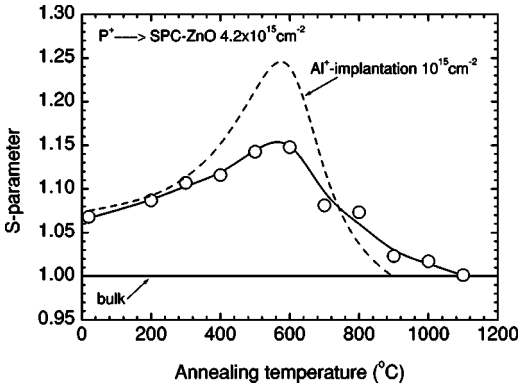

FIG. 3. Average *S* parameter in the damaged region (5–8 keV, corresponding to 0.1–0.2 μm) as a function of annealing temperature for the P^+-implanted ZnO with dose of 4.2×10^{15} cm^{-2}. The annealing behavior of Al^+-implanted sample is included for comparison.

value at 1100 °C. This implies that the number or size of the vacancies has decreased. At 1100 °C, all the detectable defects have been annealed out.

A comparison of the present result with that of the previous study of Al^+-implantation-induced defects in ZnO (Ref. 25) revealed several differences: (1) Both the positron lifetime and *S* parameter are lower for P^+ implantation (τ_2 = 343 ps and S=1.07) than for Al^+ implantation (τ_2=377 ps and S=1.08), indicating that P^+ implantation produces smaller vacancies; (2) the difference in the *S* parameter becomes larger after annealing above 400 °C. At 600 °C, the *S* parameter is much lower for the P^+-implanted sample (Fig. 3); (3) however, a higher annealing temperature is needed to remove the P^+-implantation-induced defects.

A P^+ ion is slightly heavier than an Al^+ ion, therefore, since we used the same ion dose and energy, the P^+ ion should produce more vacancies and form larger vacancy clusters. Such a contradictory circumstance can be explained by the chemical effects of ions, which affect the damage buildup and defect stability.[13] In ZnO, the strong dynamic annealing of defects occurs during ion implantation, and most of the vacancies are recovered immediately after creation. Al^+ ions might have unique chemical effects that suppress the dynamic recovery of vacancies, and much more vacancies remain after implantation. Therefore, larger vacancy clusters can be formed due to the accumulation of small vacancies. Nevertheless, the *S* parameter tends to become saturated with increasing vacancy size or concentration; therefore, the difference in the *S* parameter between these two samples is only ~0.01. After annealing, the vacancy clusters grow into microvoids with a high concentration, resulting in a very high *S* parameter in the Al^+-implanted sample. The amorphous layer is even suggested to have been induced,[25] and during recrystallization, the microvoids easily recover at temperatures that are relatively lower. For the P^+ ion, it may have a weaker stabilization effect; hence the size of the vacancy cluster is smaller. After annealing, the microvoids are possibly formed, but they have a significantly lower concentration, which is reflected by the lower *S* parameter. This suggests that the lattice structure is not likely to be amorphized by P^+ implantation. This is also confirmed by our Raman-scattering measurements, which show that ZnO lattice maintains its crystalline structure after P^+ implantation. Therefore, the annealing of the voids requires a significantly higher temperature.

Figure 4 shows the Raman spectra for the as-grown and P^+-implanted samples. For the wurtzite structure of ZnO, the Raman-active phonon modes expected from group theory are: $A_1+2E_2+E_1$,[31] where A_1 and E_1 are polar and split into transverse optical and longitudinal optical (LO) phonons with different frequencies. In our measurement range of 200–800 cm^{-1}, we observe three vibration peaks for the as-grown ZnO, which are located at 331, 437, and 575 cm^{-1}. The predominant 437-cm^{-1} peak is the high-frequency E_2 mode characteristic of the wurtzite structure, while the 331 -cm^{-1} mode is due to the multiphonon process,[31] which is twice that of the low-frequency E_2 phonon branch at the Brillouin-zone edge point (166 cm^{-1}). As for the peak at

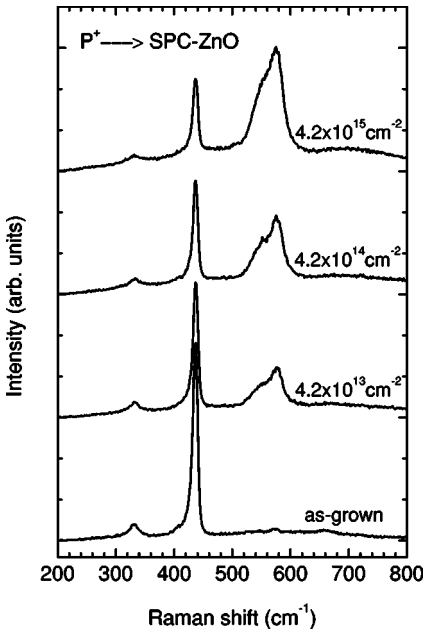

FIG. 4. Raman-scattering spectra measured for ZnO samples before and after P^+ implantation.

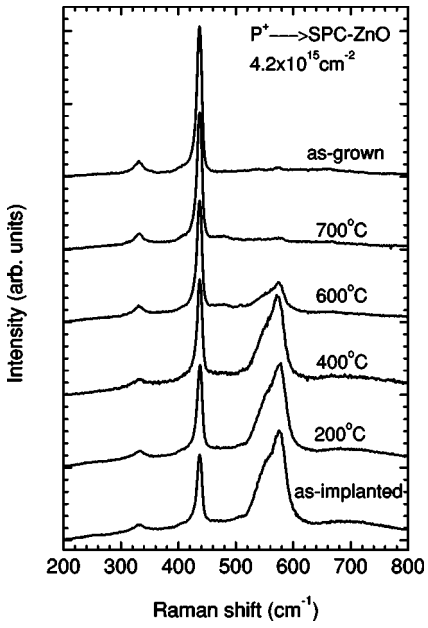

FIG. 5. Annealing effect on the Raman spectra measured for the P^+-implanted ZnO with dose of 4.2×10^{15} cm^{-2}.

575 cm^{-1}, it was ascribed by some authors as being due to either the LO phonon of A_1 (Refs. 32 and 33) or the LO phonon of E_1.[31,34,35] However, this peak might also be a defect-induced mode, and we will later discuss it in more details.

After P^+ implantation, the peak at 331 cm^{-1} barely changes. However, the peak at 575 cm^{-1} increasingly grows with an increasing dose and also becomes significantly broader (500–620 cm^{-1}). A detailed fitting of this broad peak reveals two components that are located at 560 and 578 cm^{-1}, and the low-frequency peak is significantly broader than the high-frequency peak. This broad peak is not related with the implanted phosphorus impurities, as we have also observed the same peak in the other ion-implanted or even electron-irradiated ZnO. For the LO phonon, it should become stronger in the sample with higher crystallinity, e.g., the as-grown sample. After P^+ implantation, the LO phonon band should decrease due to damage. However, we observe a contrary result. The broadband around 575 cm^{-1} increases systematically with ion implantation dose. Therefore, this broad peak should be mainly a defect-induced band. Although, the defect-induced modes are generally forbidden, they appear in defective crystals because the Raman selection rule is relaxed. Several researchers have confirmed that this band is associated with oxygen vacancies or probably Zn interstitials[33,35,36](Zn_i) because they observed its strong dependence on the oxygen stoichiometry. Therefore, we can use Raman measurements to study the oxygen vacancies produced by P^+ implantation. The strong increase of the broadband at 575 cm^{-1} indicates that a large number of V_O are created. The high concentration of V_O cut the long-range lattice ordering; therefore, the Raman selection rule is relaxed, and the Γ point phonon as well as other phonons participate in the Raman spectrum. These contribution becomes larger when the phonon-density of states is high, i.e., when the phonon-dispersion curve is relatively flat. Thus, a broad peak will appear in the Raman spectrum. In a very recent paper,[37] the same broad Raman peak was also observed in the N^+- and Ga^+-implanted ZnO, and was attributed to the damage-induced phonon mode.

The annealing effect on the Raman scattering is shown in Fig. 5. Upon annealing at temperatures below 400 °C, the broad peak at around 575 cm^{-1} shows a slight decrease, but rapidly decreases henceforth until it reaches the same level as that of the unimplanted sample at 700 °C. The E_2 peak also gradually recovers. Figure 6 shows the ratio of the integrated intensity of the broad defect peak at 575 cm^{-1} (500–640 cm^{-1}) to the sum of the 575 and 437 cm^{-1} peaks (380–640 cm^{-1}). No correction for background was made in the calculation. Initially the relative intensity of the defect peak decreases slowly with increasing annealing temperature. Above 400 °C, it begins to decrease quickly and drops to nearly the same intensity as the as-grown sample at 700 °C. It is also possible that the Zn interstitial will induce the broad phonon mode in the Raman spectrum as mentioned

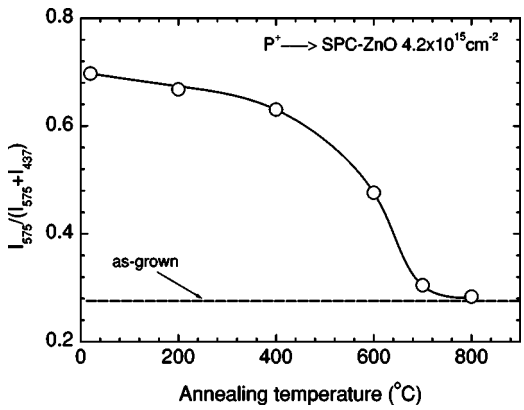

FIG. 6. Ratio of the integrated 575-cm^{-1} peak intensity to the sum of the 437 and 575 cm^{-1} peaks as a function of annealing temperature for the P^+-implanted ZnO with dose of 4.2×10^{15} cm^{-2}.

above. However this defect is expected to be annealed out at much lower temperatures than that for vacancies. A recent study by Gorelkinskii and Watkins[38] showed that electron irradiation-induced interstitials in ZnO are mobile above −163 °C and are therefore not stable at room temperature. The annealing behavior thus indicates that the broad Raman peak is not induced by Zn_i, but primarily by V_O.

The annealing result suggests that the oxygen vacancies are annealed out at ~700 °C. Such an annealing behavior differs from that of the defects probed by positrons, which prevail up to 1100 °C. In our electron-irradiated ZnO, which contains only elementary defects such as V_{Zn} and V_O, we also observed such a different annealing behavior by positron annihilation and Raman measurements. This is because oxygen vacancies are expected to be positively charged, and, consequently, they cannot trap positrons. Theoretical calculation also revealed that the positron lifetime at oxygen vacancy site is indistinguishable from the bulk lifetime.[30] Therefore, the V_O revealed by Raman is invisible to positrons. In other words, the vacancies detected by positrons, such as V_{Zn} or vacancy clusters, are not responsible for the broad Raman peak at 575 cm^{-1}. A further conclusion is that the V_O begins to migrate above room temperature, which is responsible for the agglomeration of vacancy clusters during annealing below 600 °C. By absorbing those small vacancies, the size of the vacancy clusters increases, and leads to an increase in the *S* parameter.

The Raman measurements also reveal the possible reason for the high annealing temperature of vacancy clusters induced by P^+ implantation. Though the relative height of the E_2 mode at 437 cm^{-1} decreases due to the increase of the defect-induced peak, the E_2 peak is still extremely narrow after high-dose implantation, indicating that the crystalline structure is maintained. The recovery of large vacancy clusters in the crystalline lattice thus requires a much higher temperature in comparison with that required for the large vacancy clusters in the amorphous structure, as in the case of the Al^+ implantation.[25]

B. Optical and electrical properties

Radiation-induced damage invariably affects the optical properties of semiconductors. This is particularly significant for the ion-implanted ZnO. Figure 7 shows the cathodoluminescence spectra measured for the ZnO sample before and after P^+ implantation (4.2×10^{15} cm^{-2}) and annealing. For the unimplanted ZnO, there is a band-edge ultraviolet (UV) emission peak located at 3.3 eV, which is due to the recombination of free excitons.[2,39–41] The deep level emission is rather weak and nearly invisible. Either there are few deep level centers, or there are nonradiative recombination centers that have suppressed the deep level emission.

After P^+ implantation, all the deep level and UV luminescence are completely suppressed. This is apparently due to the implantation-induced defects, and some of them act as nonradiative recombination centers, which compete with the deep level and free exciton recombination process. Annealing at low temperatures below 700 °C has no effect on the measured spectra. After annealing at 700 °C, the UV emission shows a slight recovery. This indicates that some of the nonradiative recombination centers are removed. After further annealing at 1000 °C, both the deep level and the UV emission peak increase considerably, implying that most of the nonradiative recombination centers are annealed out. At 1100 °C, the UV emission is even higher than that of the as-grown sample. This is due to the reduction in the number of nonradiative centers that exist in the as-grown sample, as proven by our previous study.[30] However, after final annealing, the deep level emission is still comparatively strong. This implies that some deep level centers prevail even after annealing. As the origin of the deep level luminescence is still under debate,[42–45] we cannot determine the remaining deep level defects. They are either implantation-induced defects or annealing-induced defects due to defect interaction at high temperatures.[46,47]

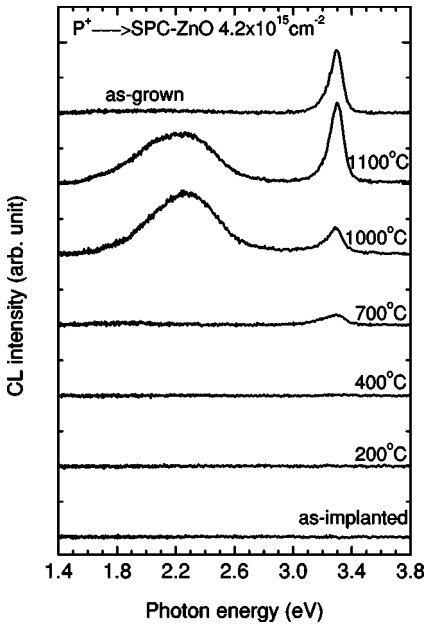

FIG. 7. Cathodoluminescence spectra as a function of annealing temperature measured for the P^+-implanted ZnO with dose of 4.2×10^{15} cm^{-2}.

The annealing of the nonradiative recombination centers, however, shows good agreement with the annealing behavior of the vacancies detected by positrons. The UV and deep level emission recover gradually from 700 °C, coinciding with the decrease in the *S* parameter shown in Fig. 3. After the disappearance of the vacancies at 1100 °C, the light emission also exhibits a full recovery. Therefore, it can be deduced that the vacancies observed by positrons might be part of the nonradiative recombination centers.

After P^+ implantation and final annealing, the implanted layer is still of the *n* type, with a sheet resistance of approximately 253 Ω/□ and an electron mobility of 87 $cm^2\ v^{-1}\ s^{-1}$. The backside of the sample, which is unimplanted and annealed at the same temperature, has a sheet resistance of 406 Ω/□. This implies that both the implanted layer and the unimplanted substrate contribute to the measured conductivity. Nevertheless, the measurement suggests that P^+ implantation enhances the *n*-type conductivity. This result is contrary to that of Kim *et al.*,[22] in which they obtained a *p*-type ZnO by doping with phosphorus. Since phosphorus is an

amphoteric dopant in ZnO,[21] the activation of this dopant into a donor or acceptor depends heavily on the thermal treatment.[22] For doping by ion implantation, the activation of phosphorus is affected by the implantation-induced defects, which can only be removed at high temperatures of 1100 °C and above. This might be the reason for the difficulty in obtaining *p*-ZnO(P). The *n*-type conduction after P^+ implantation in ZnO was also observed by Thomas *et al.* in an earlier study.[17]

IV. CONCLUSION

In conclusion, we have studied vacancies introduced by P^+ implantation in ZnO. Positron annihilation measurements reveal vacancy clusters after implantation, and they grow into a larger size after annealing below temperatures of 600 °C. Raman-scattering measurements show the production of oxygen vacancies after implantation. They disappear after annealing at ~700 °C, and are supplied for the agglomeration of large vacancy clusters. The crystalline structure of ZnO is not destroyed after implantation; therefore a high temperature of 1100 °C is required to completely remove these vacancy clusters. The P^+ implantation degrades the optical properties of ZnO to a large extent through the suppression of light emission by the nonradiative recombination centers. They are gradually recovered after annealing above 600 °C, suggesting that the vacancy defects detected by positrons are part of the nonradiative recombination centers. The P^+-implanted layer still exhibits an *n*-type conductivity. A more careful design of the implantation and subsequent annealing process is required to activate phosphorus into acceptors and remove implantation damage to avoid the degradation of optical properties.

ACKNOWLEDGMENTS

The authors would like to acknowledge the fruitful discussion with Professor Hiroshi Harima about the interpretation of the Raman-scattering data. This work was partly supported by the Nuclear Energy Generic Crossover Research Project promoted by Ministry of Education, Culture, Sports, Science and Technology of Japan.

[1] D. C. Look, D. C. Reynolds, J. R. Sizelove, R. L. Jones, C. W. Litton, G. Cantwell, and W. C. Harsch, Solid State Commun. **105**, 399 (1998).
[2] P. Zu, Z. K. Tang, G. K. L. Wong, M. Kawasaki, A. Ohtomo, K. Koinuma, and Y. Segawa, Solid State Commun. **103**, 459 (1997).
[3] D. M. Bagnall, Y. F. Chen, Z. Zhu, T. Yao, S. Koyama, M. Y. Sen, and T. Goto, Appl. Phys. Lett. **70**, 2230 (1997).
[4] K. Minegishi, Y. Koiwai, K. Kikuchi, K. Yano, M. Kasuga, and A. Shimizu, Jpn. J. Appl. Phys., Part 2 **36**, L1453 (1997).
[5] D. C. Look, D. C. Reynolds, C. W. Litton, R. L. Jones, D. B. Eason, and G. Cantwell, Appl. Phys. Lett. **81**, 1830 (2002).
[6] M. Joseph, H. Tabata, and T. Kawai, Jpn. J. Appl. Phys., Part 2 **38** L1205 (1999).
[7] A. V. Singh, R. M. Mehra, A. Wakahara, and A. Yoshida, J. Appl. Phys. **93**, 396 (2003).
[8] K. Iwata, P. Fons, A. Yamada, K. Matsubara, and S. Niki, J. Cryst. Growth **209**, 526 (2000).
[9] K. Tamura *et al.*, J. Cryst. Growth **214–215**, 59 (2000).
[10] K. Nakahara, H. Takasu, P. Fons, A. Yamada, K. Iwata, K. Matsubara, R. Hunger, and S. Niki, Appl. Phys. Lett. **79**, 4139 (2001).
[11] A. Tsukazaki, H. Saito, K. Tamura, M. Ohtani, H. Koinuma, M. Sumiya, S. Fuke, T. Fukumura, and M. Kawasaki, Appl. Phys. Lett. **81**, 235 (2002).
[12] E. Sonder, R. A. Zuhr, and R. E. Valiga, J. Appl. Phys. **64**, 1140 (1988).
[13] S. O. Kucheyev, J. S. Williams, C. Jagadish, J. Zou, C. Evans, A. J. Nelson, and A. V. Hamza, Phys. Rev. B **67**, 094115 (2003).
[14] T. Monteiro, C. Boemare, M. J. Soares, E. Rita, and E. Alves, J. Appl. Phys. **93**, 8995 (2003).
[15] F. D. Auret, S. A. Goodman, M. Hayes, M. J. Legodi, H. A. van Laarhoven, and D. C. Look, Appl. Phys. Lett. **79**, 3074 (2001).
[16] K. Ip *et al.*, Appl. Phys. Lett. **82**, 385 (2003).
[17] B. W. Thomas and D. Walsh, J. Phys. D **6**, 612 (1973).
[18] S. O. Kucheyev *et al.*, Appl. Phys. Lett. **81**, 3350 (2002).
[19] R. Krause-Rehberg and H. S. Leipner, *Positron Annihilation in Semiconductors, Defect Studies*, Springer Series in Solid-State Sciences Vol. 127 (Springer, Berlin, 1999).
[20] P. G. Coleman, *Positron Beams and their Applications* (World Scientific, Singapore, 2000).
[21] C. H. Park, S. B. Zhang, and S.-H. Wei, Phys. Rev. B **66**, 073202 (2002).
[22] K.-K. Kim, H.-S. Kim, D.-K. Hwang, J.-H. Lim, and S.-J. Park, Appl. Phys. Lett. **83**, 63 (2003).
[23] Y. W. Heo, S. J. Park, K. Ip, S. J. Pearton, and D. P. Norton, Appl. Phys. Lett. **83**, 1128 (2003).
[24] K. Ip, Y. W. Heo, K. H. Baik, D. P. Norton, S. J. Pearton, and F. Ren, J. Vac. Sci. Technol. B **22**, 171 (2004).
[25] Z. Q. Chen, M. Maekawa, S. Yamamoto, A. Kawasuso, X. L. Yuan, T. Sekiguchi, R. Suzuki, and T. Ohdaira, Phys. Rev. B **69**, 035210 (2004).
[26] J. P. Biersack and L. G. Haggmark, Nucl. Instrum. Methods **174**, 257 (1980).
[27] R. Suzuki, T. Ohdaira, and T. Mikado, Radiat. Phys. Chem. **58**, 603 (2000).
[28] T. Sekiguchi and K. Sumino, Rev. Sci. Instrum. **66**, 4277 (1995).
[29] L. J. Van der Pauw, Philips Res. Rep. **13**, 1 (1958).
[30] Z. Q. Chen, S. Yamamoto, M. Maekawa, A. Kawasuso, X. L. Yuan, and T. Sekiguchi, J. Appl. Phys. **94**, 4807 (2003).
[31] T. C. Damen, S. P. S. Porto, and B. Tell, Phys. Rev. **142**, 570 (1966).
[32] X. Wang, S. Yang, J. Wang, M. Li, X. Jiang, G. Du, X. Liu, and R. P. H. Chang, J. Cryst. Growth **226**, 123 (2001).
[33] C. J. Youn, T. S. Jeong, M. S. Han, and J. H. Kim, J. Cryst. Growth **261**, 526 (2004).
[34] Y. J. Xing *et al.*, Appl. Phys. Lett. **83**, 1689 (2003).
[35] J. N. Zeng, J. K. Low, Z. M. Ren, T. Liew, and Y. F. Lu, Appl. Surf. Sci. **197**, 362 (2002).
[36] M. Tzolov, N. Tzenov, D. Dimova-Malinovska, M. Kalitzova, C. Pizzuto, G. Vitali, G. Zollo, and I. Ivanov, Thin Solid Films **379**, 28 (2000).
[37] F. Reuss, C. Kirchner, Th. Gruber, R. Kling, S. Maschek, W. Limmer, A. Waag, and P. Ziemann, J. Appl. Phys. **95**, 3385 (2004).
[38] Y. V. Gorelkinskii and G. D. Watkins, Phys. Rev. B **69**, 115212 (2004).
[39] T. Sekiguchi, N. Ohashi, and Y. Terada, Mater. Sci. Forum **258–263**, 1371 (1997).
[40] N. Ohashi, T. Sekiguchi, K. Aoyama, T. Ohgaki, Y. Terada, I. Sakaguchi, T. Tsurumi, and H. Haneda, J. Appl. Phys. **91**, 3658 (2002).
[41] D. W. Hamby, D. A. Lucca, M. J. Klopfstein, and G. Cantwell, J. Appl. Phys. **93**, 3214 (2003).
[42] K. Vanheusden, C. H. Seager, W. L. Warren, D. R. Tallant, and J. A. Voigt, Appl. Phys. Lett. **68**, 403 (1996).
[43] D. C. Reynolds, D. C. Look, B. Jogai, J. E. Van Nostrand, R. Jones, and J. Jenny, Solid State Commun. **106**, 701 (1998).
[44] B. Lin, Z. Fu, and Y. Jia, Appl. Phys. Lett. **79**, 943 (2001).
[45] N. Y. Garces, L. Wang, L. Bai, N. C. Giles, L. E. Halliburton, and G. Cantwell, Appl. Phys. Lett. **81**, 622 (2002).
[46] H. S. Kang, J. S. Kang, S. S. Pang, E. S. Shim, and S. Y. Lee, Mater. Sci. Eng., B **102**, 313 (2003).
[47] T.-B. Hur, G. S. Jeen, Y.-H. Hwang, and H.-K. Kim, J. Appl. Phys. **94**, 5787 (2003).